E3S Web of Conferences **479**, 05002 (2024) https://doi.org/10.1051/e3sconf/202447905002
ISSAT 2023

Experimental study on effect of superheat degree in an organic Rankine cycle with a scroll expander

Yi-Chi Hsieh[1*], *Yen-Hsun* Chen[1], and *Jui-Ching* Hsieh[1]

[1]National Chin-Yi University of Technology, Department of Mechanical Engineering, Taichung City, Taiwan

Abstract. A micro-organic Rankine cycle (ORC) system utilizing R134a as the working fluid and a scroll expander has been developed. In this study, the effects of superheat degree on system performance were investigated by varying the evaporation temperature and refrigerant mass flow rate. The heat sources used in the ORC system were three different temperatures: 85℃, 95℃, and 105℃. The results indicate that the refrigerant mass flow rate increases with the rise in evaporation pressure, while superheat degree decreases. Moreover, higher superheat degrees led to a reduction in the system power generation. The trend of net efficiency demonstrates that when superheat degree increases, the net efficiency first rises to a peak before declining. At heat source temperatures of 85℃, 95℃, and 105℃, the peak net efficiencies are 4.86%, 5.56%, and 5.87%, respectively, with corresponding superheat degrees of 25.72K, 36.16K, and 38.15K.

1 Introduction

With the rapid development of global industrialization, energy scarcity has emerged as a significant challenge facing the world. Based on survey data [1], approximately 20% to 50% of industrial waste heat is lost to the environment, and low-temperature waste heat (< 200°C) makes up as much as 55% of this proportion. Consequently, the effective utilization of energy has become an urgent issue that needs a solution. In this context, this technology offers a promising solution by converting medium to low temperature thermal energy into electricity. ORC is applicable not only application in renewable energy systems but also plays a crucial role in industrial process waste heat recovery. It combines features of environmental sustainability, high reliability, and electricity generation without reliance on high-temperature energy sources, making it a cost-effective green energy-saving innovation. Until now, the ORC technology has been applied to various thermal energy sources, including solar [2], biomass [3], and geothermal [4,5].

When designing an ORC system, it is crucial to conduct a comprehensive investigation of several critical parameters, such as heat source temperature, evaporation pressure (P_{eva}), mass flow rate ($\dot{m}_{wf}$), and superheat degree (T_{sh}), to achieve the optimal performance of ORC. Peris et al. conducted experiments on the performance of the ORC system within the

* Corresponding author: kiwibaby0205@gmail.com

range of heat source temperature from 90 °C to 150 °C. Their result shows that increasing the heat source temperature and pressure ratio effectively enhances both power generation and efficiency [6]. Zhou et al. conducted experiments to study the relationship between system performance and evaporation pressure, heat source temperature, and superheat degree. The results indicated that the T_{sh} increased with an increase in the T_{hs}, negatively affecting system performance and power generation [7]. Liu et al. investigated the sensitivity of ORC system performance to various system parameters such as working fluid, superheat degree, and evaporating temperature. Their results indicated that the evaporation temperature significantly influences both the performance and economics of the ORC system [8]. Chang et al. investigated the performance of a scroll expander by varying the superheat degree at the expander inlet and the system pressure differential. Their experimental results revealed that, at a fixed rotational speed, increasing superheat degree led to improvements in isentropic efficiency and system efficiency, reaching maximum values of 72.2% and 8.12% respectively [9].

Although numerous studies have focused on the optimization and analysis of system parameters, there are a few literatures to examine effect of superheat degree on the system performance under the different low-temperature heat sources. Therefore, to address the research gap, this study developed a micro-ORC experimental device that utilizes a scroll expander, employing R134a as the working fluid. The study aims to investigate the effect of superheat degree on the system's performance, considering a range of low-grade heat sources with temperatures ranging from 85 to 105°C in intervals of 10 K.

2 Methodology

2.1 Experimental device

The ORC experimental device setup was constructed in the lab. Comprising a working fluid pump, the heat exchanger (evaporator and condenser), and an expander, the schematic diagram of ORC device is shown in Fig. 1(a). The working fluid (WF) enters from Site 1 to Site 2, being pressurized through the working fluid pump before entering the evaporator. From Site 2 to Site 3, the liquid WF absorbs heat from the external heat source within the evaporator, transforming into a superheated vapor (or saturated vapor), which is then flowed to the expander. During the transition from Site 3 to Site 4, the high-temperature, high-pressure vapor WF undergoes pressure reduction and expansion across the expander. This transformation effectively converts the pressure differential into the mechanical kinetic energy of the expander, subsequently driving the generator for electricity output. Moving from Site 4 to Site 1, the vapor WF at low pressure, having completed a work process, is then directed to the condenser. It releases heat and transitions into a liquid state and is subsequently directed back to the working fluid pump, thus completing a thermodynamic cycle. The system employed R134a as WF, and the expander unit has been modified from a scroll compressor. Fluid properties are referenced from NIST REFPROP 9.0. Relevant components and sensors were selected according to design criteria and the system was constructed. The system dimensions: Width:120 cm, Height:248 cm, Length:165 cm. The schematic diagram of ORC and the detailed 3D diagram are shown in Fig. 1.

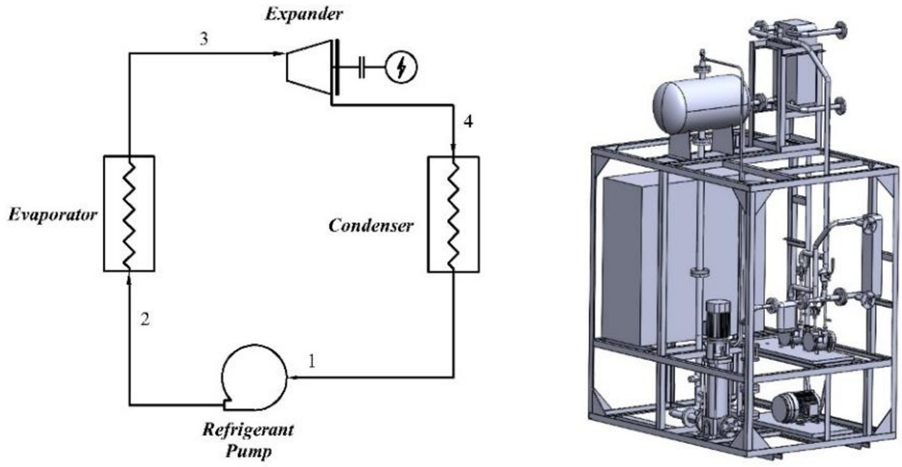

(a) (b)

Fig. 1. ORC experimental device: (a) schematic and (b) 3D diagrams.

Additionally, this study utilizes an industrial boiler to heat the water in the heating loop for simulating heat sources from waste heat. The industrial boiler has a heat generation capacity of up to 800 kW, and its temperature can be adjusted using control panels to meet the pre-set temperature requirements.

2.2 Data reduction

This study conducts thermal analysis on the individual components of the ORC to compute their performances and determine the performance of the ORC. A pump pressurizes the WF before it enters the evaporator during operation, where it absorbs heat and transforms into a vapor state. The heat capacity in the evaporator is evaluated as follows [10]:

$$Q_{\mathrm{eva}} = \dot{m}_{\mathrm{wf}}(h_{\mathrm{eva,out}} - h_{\mathrm{eva,in}}) \quad (1)$$

where $h_{\mathrm{eva,in}}$ denotes the enthalpies at the evaporator inlet, and $h_{\mathrm{eva,out}}$ denotes the enthalpies at the evaporator outlet. To prevent the WF from entering the expander in a liquid state, it is crucial to maintain an appropriate superheat degree (T_{sh}) at the evaporator outlet. Which is defined as the temperature difference between the expander inlet temperature ($T_{exp,in}$) and the evaporation temperature (T_{eva}), and it is calculated as follows [11]:

$$T_{\mathrm{sh}} = T_{\mathrm{exp,in}} - T_{\mathrm{eva}} \quad (2)$$

As the gaseous WF enters the expander, it expands, generating energy (W_{exp}) that drives the rotation of the generator, leading to the production of electrical power (W_{elec}). It's important to consider the efficiency of the generator in this process [10].

$$W_{\mathrm{exp}} = \dot{m}_{\mathrm{wf}}\left(h_{\mathrm{exp,in}} - h_{\mathrm{exp,out}}\right) = \frac{W_{\mathrm{elec}}}{\eta_{\mathrm{gen}}} \quad (3)$$

where $h_{\mathrm{exp,in}}$ is the enthalpies at the inlet of the expander, and $h_{\mathrm{exp,out}}$ is the enthalpies at the outlet of the expander. The calculation for the ORC's net efficiency (η_{net}) is as follows [12]:

$$\eta_{\mathrm{net}} = \frac{W_{\mathrm{net}}}{Q_{\mathrm{eva}}} = \frac{W_{\mathrm{exp}} - W_{\mathrm{p}}}{Q_{\mathrm{eva}}} \quad (4)$$

where W_p is the power consumption measured by the working fluid pump, and it can be expressed: [13]:

$$W_p = \dot{m}_{wf}\left(h_{p,out} - h_{p,in}\right) \quad (5)$$

where $h_{p,out}$ is the enthalpies of the pump outlet, and $h_{p,in}$ are the enthalpies of the pump inlet.

3 Results and discussion

To control the P_{eva} and $\dot{m}_{wf}$ in the ORC device, a variable frequency drive (VFD) has been installed, which is controller of the working fluid pump. The P_{eva} increased when the VFD frequency raised, resulting in a corresponding increase in $\dot{m}_{wf}$. The effect of the P_{eva} on the T_{sh} is shown in Figure 2(a). It can be found that the T_{sh} decreased with an increase in P_{eva}. This is because higher P_{eva} corresponded to higher evaporation temperature at a given heat source temperatures, consequently leading to a decrease in T_{sh}. Moreover, for a given P_{eva}, the T_{sh} increased with an increase of the heat source temperatures [18]. Fig. 2(b) shows the effect of the $\dot{m}_{wf}$ on the T_{sh}. The $\dot{m}_{wf}$ was directly proportional to the P_{eva}, but inversely proportional to the T_{sh} [14].

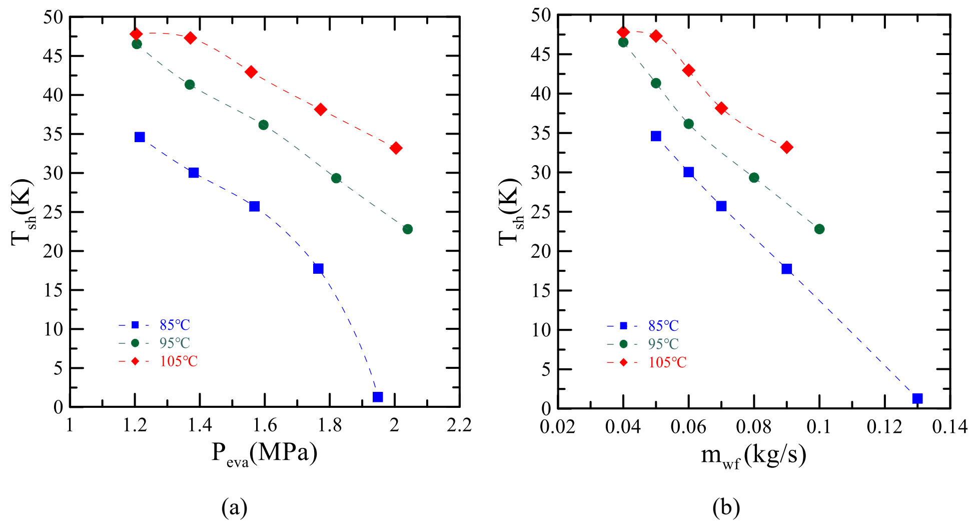

Fig. 2. Effect of (a)evaporation pressure and (b) mass flow rate on superheat degree.

The effect of T_{sh} on system performance is illustrated in Fig. 3. From Fig. 3(a), it is evident that an increase in T_{sh} had a negative effect on power generation. There are two reasons for this effect. First, when the T_{sh} increased [7,14], the amount of heat absorbed by the working fluid from the heat source decreased [15]. Second, when the $\dot{m}_{wf}$ decreased, the T_{sh} increased. However, the power generation decreased with a decrease in $\dot{m}_{wf}$ [7]. Figure 3(b) indicated the T_{sh} effect on the system's net efficiency under three different heat source temperatures. The net efficiency initially increases and then decrease as the heat source temperature increases [7,16]. At heat source temperatures of 85°C, 95°C, and 105°C, the peak net efficiencies were 4.86%, 5.56%, and 5.87%, respectively, with corresponding T_{sh} of 25.72K, 36.16K, and 38.15K.

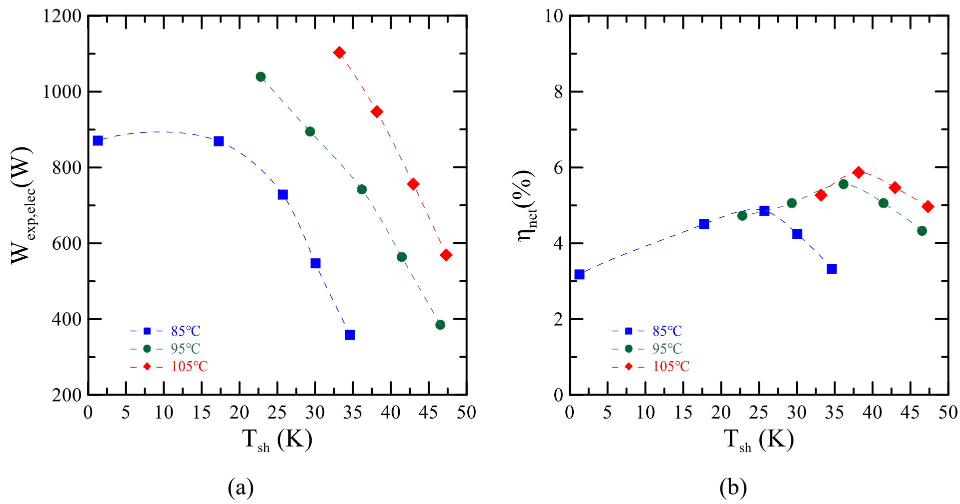

Fig. 3. Effect of superheat degree on (a) power generation and (b) net efficiency.

4 Conclusion

This research investigated the performance of the ORC device with a scroll expander using R134a as WF. The effect of the T_{sh} on system performance under three different heat source temperatures including the net efficiency and power generation were researched. The main conclusions can be summarized as follows:

a. The P_{eva} and $\dot{m}_{wf}$ were regulated by a VFD, and both increased with an increase of frequency [10].

b. The T_{sh} decreased with an increase of P_{eva} [17]. This was because, for a given heat source temperature, higher P_{eva} resulted in a higher evaporation temperature, thus reducing the T_{sh}. Furthermore, increasing the heat source temperature while maintaining a constant P_{eva} resulted in a higher T_{sh}.

c. The higher T_{sh} resulted in a decrease in power generation. This was because increased T_{sh} reduces the amount of heat absorbs from the heat source, which decrease power generation [7,14,17], It can be inferred that a high T_{sh} has a negative effect on the power generation.

d. The peak net efficiencies at heat source temperatures of 85°C, 95°C, and 105°C were 4.86%, 5.56%, and 5.87%, corresponding to T_{sh} of 25.72K, 36.16K, and 38.15K, respectively.

The authors gratefully acknowledge the financial support from the National Science and Technology Council of Taiwan under grant numbers NSTC 108-2221-E-167-007-MY3 and NSTC 111-2221-E-167-017-MY3.

References

1. Reported new record temperature of 38°C north of Arctic Circle. World Meteorological Organization (WMO).
2. B. F. Tchanche., Appl Therm Eng, **29**, 2468-2476, (2009).
3. L. A. Prananto., Appl Therm Eng, **132**, 686-696, (2018).
4. N. F. Shokati, M. Ranjbar. Yari., Renew Energ, **83,** 527-542, (2015).

5. A. Ahmadi., J Clean Prod, **274**, 122950, (2020).
6. B. Peris, J. Navarro-Esbrí, F. Molés, M. González, A. Mota-Babiloni., Energy, **82**, 269-276, (2015).
7. N. Zhou, X. Wang, Z. Chen, Z. Wang., Energy, **55**, 216-225, (2013).
8. X. Liu, X. Wang, C. Zhang., Appl Therm Eng, **71**, 175-183, (2014).
9. J.C. Chang, T.C. Hung, Y.L. He, W. Zhang., Appl Energ, **155**, 150-159. (2015).
10. J. C. Hsieh, Y. H. Chen, Y. C. Hsieh., Energy, **270**, 126956, (2023).
11. X. Zheng, X. Luo, J. Luo, J. Chen, Y. Liang, Z. Yang, H. Wang., Energ Convers Manage, **207**, 112528, (2020).
12. A. Kheiri, M. Feidt, S. Pelloux-Prayer., Energy, **78**, 622-638, (2014).
13. Y.M. Li, T.C. Hung, C.J. Wu, T.Y. Su, H. Xi, C.C. Wang., Energy, **217**, 119342, (2021).
14. Y. Zhou, J. Ruan, G. Hong, Z. Miao., Energies, 15, 5505, (2022).
15. Prasetyo. T, Surindra. MD, Caesarendra. W, Taufik. Glowacz. A, Irfan. M, Glowacz. W., Symmetry, **12**, 1463, (2020).
16. C. Campana, L. Cioccolanti, M. Renzi, F. Caresana., Energy, **187**, 115929, (2019).
17. Ziviani. D, Gusev. S, Lecompte. S., Groll. EA, Braun. JE, Horton. WT, De Paepe. M., Appl Energ, **189**, 416-432, (2017).
18. Guo. C, Du. X, Yang. L, Yang. Y., Appl Therm Eng, **75**, 135-144, (2015).